A new test setup for studying sand behaviour inside an immersed tunnel joint gap

Rheza Rahadian, Rheza; van der Woude, Sallo; Wilschut, D.; Blom, Kees; Broere, Wout

DOI
10.1201/9780429438660-63

Publication date
2018

Document Version
Final published version

Published in
Physical Modelling in Geotechnics

Citation (APA)
Rheza Rahadian, R., van der Woude, S., Wilschut, D., Blom, K., & Broere, W. (2018). A new test setup for studying sand behaviour inside an immersed tunnel joint gap. In A. McNamara, S. Divall, R. Goodey, N. Taylor, S. Stallebrass, & J. Panchal (Eds.), *Physical Modelling in Geotechnics* (pp. 443–448). Taylor & Francis. https://doi.org/10.1201/9780429438660-63

Physical Modelling in Geotechnics – McNamara et al. (Eds)
© 2018 Taylor & Francis Group, London, ISBN 978-1-138-34419-8

A new test setup for studying sand behaviour inside an immersed tunnel joint gap

R. Rahadian
Delft University of Technology, Delft, The Netherlands

S. van der Woude
Van Hattum en Blankevoort, Woerden, The Netherlands

D. Wilschut
Municipality of Rotterdam, The Netherlands

C.B.M. Blom & W. Broere
Delft University of Technology, Delft, The Netherlands

ABSTRACT: During inspections of several immersed tunnels in the Netherlands, damage of immersion joints has been observed. In some cases the Gina seal has moved inwards from its original location, and in other cases a permanent elongation of the entire tunnel structure has been measured. For both cases it has been hypothesised that a seasonal expansion and contraction of the tunnel elements allows sand to enter the joint gap between elements during winter, where it is compacted during summer, leading to an increasing amount of sand in the joint gap over the years. In order to study this mechanism and assess its impact, a 1:3 scale model joint gap has been designed and constructed. This setup can simulate expansion and contraction cycles of the joint and measure stresses in the joint gap and deformations of the Gina seal. First test results are presented here and show that compaction of the sand entering the joint gap indeed occurs and leads to the observed large inwards deformations of the Gina seals.

1 INTRODUCTION

Immersed tunnels are constructed from several elements which are immersed next to each other and joined together by making an immersion joint, which forms the temporary and permanent watertight connection between elements (Lunniss and Baber 2013). The most common immersed tunnel design uses thick-walled concrete shells for the tunnel construction and a double rubber seal to waterproof the immersion joint. The roughly trapezoid shaped Gina seal consists of 2 main parts, the stiff base and the soft nose that will compress once the elements are lined up to one another. It is bolted to the concrete shell of the tunnel on one side of the joint and compressed during the immersion procedure. According to the immersed tunnel design guidelines this serves as a temporary seal (COB Commissie T202 2015). The Omega seal is a curved rubber strip placed around the inner side of the immersed joint after the water between the bulkheads have been drained. It functions as the secondary measure against leakage and is intended as the permanent seal. See Figure 1 for a sketch of the immersion procedure and Figure 2 for a detail of the joint and seals.

The Gina gasket compresses due to the water pressure at the far bulkhead of the element during immersion, but a gap between the end frames remains, as shown in Figure 2. The gap allows for water and soil to enter after the soil cover has been backfilled on top of the tunnel.

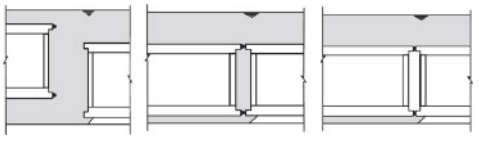

Figure 1. Construction procedure of immersion joint.

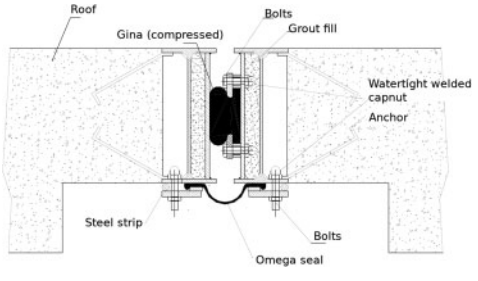

Figure 2. Gina and Omega seal solution in an immersed tunnel joint.

During regular inspections of several immersed tunnels in the Netherlands damage has been observed at immersion joints, and in some occasions an increasing elongation of the entire tunnel has been observed over the years. It has also been observed that the tunnel elements expand during summer and contract during winter, resulting in a seasonal contraction-expansion of the immersion joint (Berkhout 2015). These observations have led to the hypothesis that during expansion soil enters into the gap and is compressed during joint contraction. The seasonal contraction-expansion may lead to failure of the soil mass in the joint, densifying the soil in the joint gap and applying an increasing pressure on the outside of the Gina seal.

The Gina seal is not intended to withstand high loads on the outside. In one occasion it was observed that the Gina gaskets punched through the inner side of the tunnel joint and damaged the Omega gaskets. This not only implies an increased pressure on the outside of the Gina, but also failure of the bolts by which it is attached to the tunnel structure, and a continued inflow of soil into the joint gap as the Gina gradually moves downward. As finite element simulations were unable to prove the exact failure mechanism occurring in the joint gap and reliably estimate the pressure exerted by the soil on the Gina, a scale model of the joint gap has been designed to study the behaviour of the Gina during seasonal compression-expansion cycles.

2 EXPERIMENTAL SETUP

2.1 *Design considerations and test setup*

The test setup is intended as a physical model of the outer side of the immersed joint gap. It is divided into 2 main parts:

- the top part (a) models the soil column outside of the joint gap. The soil column is put inside a tubular drum container with an opening at the bottom that connects it to the bottom part. The stress conditions in the drum should be controlled to resemble the overburden above the tunnel.
- the bottom part (b) models the immersed joint gap, which is rectangular shaped. This section houses the Gina profile pushed against the tunnel structure and a mechanical jack that allows it to move in a cyclic motion, to simulate expansion-contraction throughout the seasons.

The entire setup is contained in a rectangular metal frame with two rings bolted to the sides around mid height at the center of gravity. These rings allow the entire setup to be lifted by a crane and flipped over.

After considering scaling effects and the expected forces in the model setup, a model scale of 1:3 has been chosen. A side view sketch of the equipment is shown in Figure 3, which shows the soil drum containing soil and an inflatable bladder that can be filled with air to simulate a vertical overburden pressure, the fixed wall on the left to which the Gina profile is attached and the movable wall on the right. The latter is attached to a

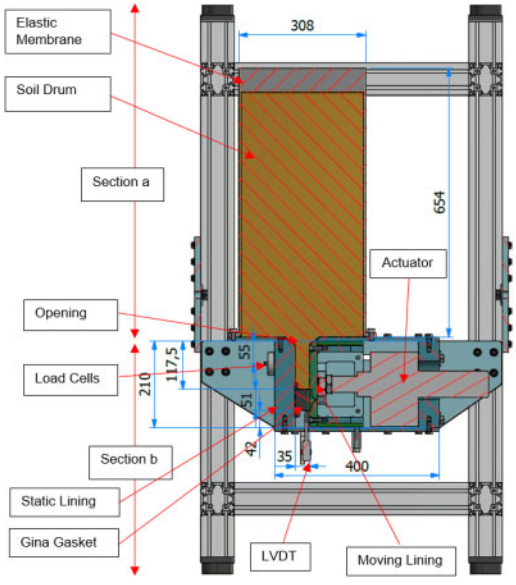

Figure 3. Cross-section of the test equipment.

mechanical jack (Madler 50 kN), which is used to close the joint gap and compress the Gina in its initial position and simulate the seasonal contraction-expansion. In addition two load cells (Burster type 8523-100) are mounted on the fixed wall with modified 10 mm diameter load plates positioned flush with the joint wall and in contact with the soil. A LVDT (ELE 10) is placed on the bottom side of the Gina seal.

The top edges of the lining are slightly curves, to mimic the actual tunnel structure. This small detail might further facilitate the densification process as the soil easily intrudes into the gap when the joint expands.

In addition, there are two 7 mm diameter openings in the opposing side walls of the joint gap (perpendicular to this cross-section) at the center height of the load cells, which allow a pocket penetrometer access to the soil in the gap.

2.2 *Model Gina profile*

The model Gina gasket (Figure 4) used in this experiment is supplied by Trelleborg, the manufactrer of most Gina seals used in immersion projects. The gasket is molded out of a similar type of material compared to the original gasket, albeit with lower elastic modulus to compensate for the limitations of the actuator. The elastic modulus of the gasket is at 1.0 MPa, whereas the a Gina profile made in the regular Sh-50 quality would have a 2.2 MPa elastic modulus.

However, as the Gina gasket is made out of similar rubber material, the Poissons ratio of the model gasket is comparable to the prototype at $\nu = 0.498$. The high Poissons ratio implies that the gasket is nearly incompressible, and any axial compression is translated into lateral extension.

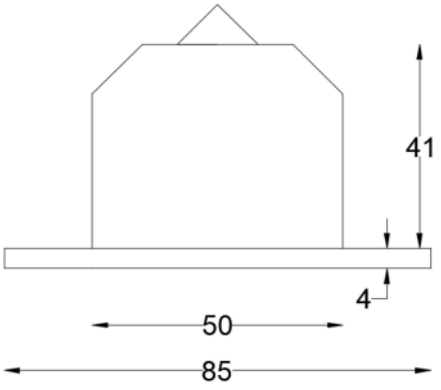

Figure 4. Model Gina seal.

2.3 *Modified penetrometer*

Various authors have correlated penetrometer resistance to soil density. A commonly used relationship is Kulhawy & Mayne (1990), which takes into account the overconsolidation ratio of the soil. The relative density is derived from

$$D_r^2 = \frac{Q_{cn}}{305 Q_C Q_{OCR}} \tag{1}$$

where

$$Q_{cn} = \frac{\left(\frac{q_c}{p_a}\right)}{\sqrt{\left(\frac{\sigma'_v}{p_a}\right)}} \quad ; \quad Q_{OCR} = OCR^{0.18} \tag{2}$$

and Q_C is a compressibility factor, which is 0.91 for high, 1.0 for medium and 1.09 for low compressible soils.

Jamiolkowski (2001) modified the relationship from Kulhawy & Mayne (1990) to

$$D_r(\%) = 26.8 \ln Q_{cn} - b_x \tag{3}$$

where b_x takes values of 52.2, 67.5 and 82.5 for high, medium and low compressible soils respectively.

Schmertmann (1976) obtained a different correlation

$$D_r = \frac{100}{C_2} \ln \frac{q_c}{C_0 (\sigma'_{v0})^{C_1}} \tag{4}$$

where suggested values for a number of normally consolidated sand are $C_0 = 0.050$, $C_1 = 0.700$ and $C_2 = 2.91$ (Sandrekarimi 2016).

These relations are based on results from cone penetrometer tests, but the size of the model joint does not allow the use of a full-scale 10 cm^2 CPT cone. Instead a scaled penetrometer will be used, based on a modified Eijkelkamp 500 kPa pocket penetrometer. This device has a rod diameter of 0.25" which is small enough to be used in the joint gap. However, in its unmodified state, the effective penetration depth is only 10 mm. Therefore, the rod is extended to provide a 70 mm effective penetration depth, as shown in Figure 5.

Figure 5. Modified pocket penetrometer.

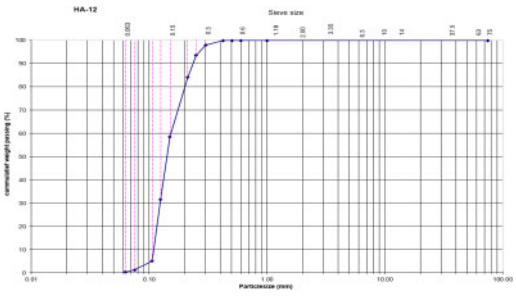

Figure 6. Grain size distribution.

The pocket penetrometer only records the cone resistance q_c, as the sleeve area is considered to be too small to contribute to friction, and the device itself usually lack the means of measuring friction resistance. Due to the extended probe length, some friction resistance is may contribute to the readings, but this is not corrected for.

A further point is that the penetrometer is normally used in a vertical penetration direction. In this setup, however, the penetrometer will be inserted horizontally. Research on horizontal cone penetration conducted by Broere & van Tol (1998) and Broere (2001) produced a relationship between vertical and horizontal cone resistances, indicating that depending on the sand density, a deviation between horizontal and vertical CPT readings might occur. Based on cavity expansion theory, a ration of $q_{c,hor}/q_{c,ver}$ up to 1.5 might occur for medium dense sand with $K = 0.5$. This correction for the horizontal orientation has been included in the derivation of relative densities in Table 2.

2.4 *Sand properties*

The sand used in the tests is a mixture of Geba Weiss (a fine sand with D_{50} of 100 μm) and medium sized fractions of Maas river sand (sieve openings between 125 and 250 μm) in a ratio of 80/20, to obtain a distribution closely resembling field conditions, see Figure 6.

The resulting sand has a dry volumetric weight γ_d of 17 kN/m^3 and minimum and maximum void ratio have been determined as 0.548 and 0.929 respectively (Elmi Anaraki 2008).

2.5 *Test procedure*

The experimental procedure consist of a preparation and execution stage. During the preparation phase the

Table 1. Summary of test series.

Test	Test Code	Overburden (kPa)	Stroke (mm)	No. of Cycles
Calibration Tests				
Zero cycle	TC1-XX	68	0	0
Stepwise penetrometer	TC2-XX	68	3.5	50
Sandless test	TC3-YY-XX	0	Varies	25
Main Series				
Reference (1.5 mm)	TVS15-XX	68	1.5	25
0.5 mm stroke	TVS05-XX	68	0.5	75
1.0 mm stroke	TVS10-XX	68	1.0	50
2.5 mm stroke	TVS25-XX	68	2.5	20
3.5 mm stroke	TVS35-XX	68	3.5	10

entire setup is initially in a flipped position, with the soil drum on the bottom side. The air bladder in the drum is not pressurized. The entire setup is rattled while suspended to ensure no soil remains in the joint gap and the soil in the drum is in a loose state. After this the joint gap is closed to a 35 mm gap size. Next, the entire setup is gently flipped over, so the soil drum is in top position, and lowered to the ground. Finally, the air bladder is inflated to the desired pressure of 58 kPa. Including the weight of the soil column this results in a 68 kPa overburden pressure at the top of the joint gap.

Prior to starting the actual test, a penetrometer reading is taken at one side of the joint. The cyclic deformation of the joint is started by a half-range outward (expansion) of the joint, followed by the desired number of full range compression-expansion cycles. Normally, at the end of the full series of loading-unloading cycles, a second penetrometer reading is taken, at the other side, the side not previously disturbed by the first penetrometer reading.

In addition to this regular test schedule, a number of tests have been performed for calibration purposes. These include tests where the penetrometer readings were taken at both sides, without performing any loading-unloading cycles at all. These tests serve to show the resistance of the newly loosened sand after each test setup reset.

In a different calibration test, penetrometer readings were taken after each 5 loading-unloading cycles. During each penetrometer measurement, the probe is inserted into the soil to a depth of 7 cm. This action might locally disturb the soil inside the joint gap and provide false readings if subsequent tests are made at the same side without resetting the test setup.

Finally, a series of tests has been performed without soil in the setup. These tests serve to investigate the deflection of the Gina during subsequent compression-extension cycles, in order to verify that without a soil load on the outside, the Gina expands downwards during compression due to its near incompressibility, and fully bounced back during unloading.

The expansion and contraction cycle of the joint gaps depends on the tunnel material, the length of each

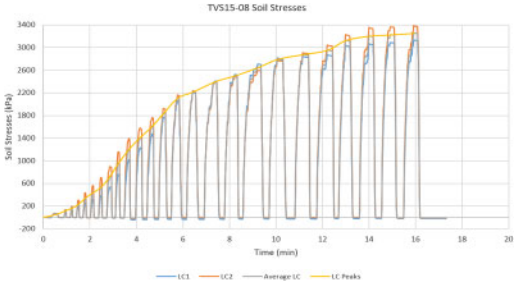

Figure 7. Soil stresses measured in TVS15-08.

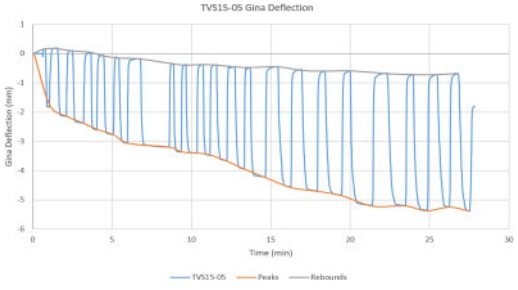

Figure 8. Gina gasket deflection during TVS15-05.

element and the seasonal temperature variation. The prototype tunnel joints contract and expand a maximum of 10 mm throughout the years. In the model would this translates to max. 3.5 mm deformation cycles. However, as the capacity of the screw jack is limited, the reference stroke length used will be 1.5 mm for 50 cycles. In test variations 0.5, 1.0, 1.5, 2.5 and 3.5 mm will be used, although it proved to be necessary to limit the number of loading cycles at larger stroke lengths due to the limitations of the screw jack. This results in the test configurations listed in Table 1.

3 RESULTS

Graphs for some test results are shown below. Figure 7 shows the load cell measurements for TVS15-08. The results from both load cell, indicated by LC1 and LC2 are averaged and a line connecting the subsequent peak stresses at the end of each compression stage. The increase of the stress in the joint after each cycle is visible. The rate of stress increase drops off in later cycles, but no clear limit is reached during the first 27 cycles.

Figure 8 shows the downward deflection and rebound of the Gina during TVS15-05. A line is included that connects the peak downward deformation at the end of each compression cycle, as well as a line connection the remaining deformation after rebound at the end of each extension cycle. It is clear that the Gina gasket moves increasingly downwards at the end of each compression cycle, and does not fully rebound to its initial position after relaxation.

Figure 9 shows the results for sandless control test TC3-15-01, which has the same 1.5 mm stroke length

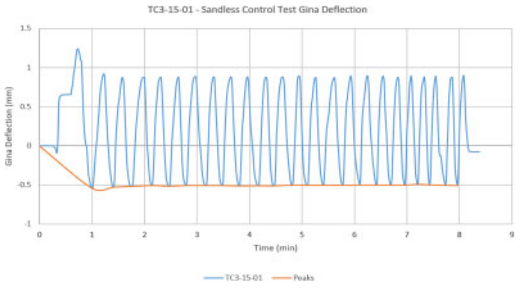

Figure 9. Gina gasket deflection during TC3-15-01 (1.5 mm deflection sandless control test).

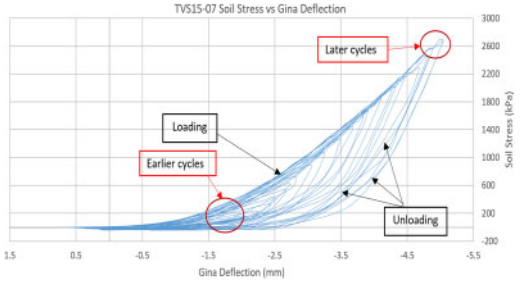

Figure 10. Soil stresses vs. Gina deflection for TVS15-07.

as TVS15-05. It can be observed that without the influence of the sand, both the gasket deflection peak and rebound points remains relatively constant throughout the test despite a too large unloading stroke in the first cycle and small inaccuracies in subsequent strokes. Comparing the gasket deflection values of both graphs shows that the sand has a significant effect on the overall gasket deflection.

Figure 10 plots the averaged soil stress (measured in the horizontal direction) versus the vertical deflection of the Gina gasket over the entire loading cycle. It can be observed that during the loading part of every cycle, the system follows a certain gradient. However, hysteretic behaviour is present during unloading, where the stress relief is much more rapid compared to the rebound of the Gina gasket. The hysteretic behaviour is more apparent at later cycles and at higher gasket deflections, with more pronounced lagging of gasket rebound compared to the stress decrease.

Figure 11 shows the peak deflection point graphs for every configuration normalized with their respective stroke lengths. It can be observed that the deflection results for equal stroke lengths are similar. This shows the reliability of the test setup, and signifies that the soil in the joint gap demonstrates similar behaviour at similar load conditions.

However, observing results for different stroke lengths reveals that the gradient of the peak points lines differ from each other. The curve becomes steeper as the stroke length increases. This suggests that the soil undergoes escalating plastic deformations, which allows more soil to enter the joint gap, increasing the soil density in the gap and propagating the effect.

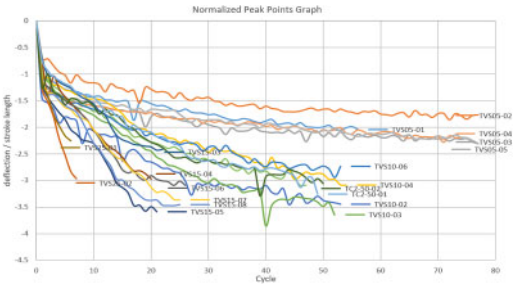

Figure 11. Normalized peak deflection points for all tests.

Table 2. Relative densties derived from test results.

Test	No. of cycles	D_r (%) Start[1]	End[1]	End[2]
TVS05-01	56	4.7	29.3	43.2
TVS05-02	77	3.5	23.9	37.8
TVS05-03	77	4.7	27.1	41.0
TVS05-04	74	0	26.3	40.2
TVS05-05	77	0	23.0	36.9
TVS10-02	53	0	25.0	38.9
TVS10-03	52	4.7	22.4	36.3
TVS10-04	54	0	23.4	37.3
TVS10-05	47	0	24.6	38.5
TVS10-06	53	0	24.4	38.3
TVS15-01	5			
TVS15-02	20			
TVS15-03	22			
TVS15-04	20	0.3	30.4	44.3
TVS15-05	21	0	27.1	41.0
TVS15-06	26	0	18.3	32.2
TVS15-07	25	0	17.4	31.3
TVS15-08	25	0	14.0	27.9
TVS25-01	7	0	17.4	31.3
TVS25-02	7	0	14.0	27.9

[1] Lower estimate: corrected for horizontal test direction.
[2] Upper estimate: not corrected for stress conditions.

Figure 12 visualises the penetrometer test results shown in Table 2. Results with similar stroke lengths were grouped and at rend line was drawn. Similar to the stress increase discussed above, the trend line results also show an increase in gradient with increasing stroke lengths. This signifies a greater rate of densification at higher strains. Even for the highest penetrometer resistances plotted here, the derived relative density remains at 30%, which would be categorized as a medium low to medium dense sand. This is, however, after the final relaxation cycle, which still means that overall significant and permanent densification has taken place. Also, the results of TVS05 and TVS10 tests show that the cone resistance values continue to increase well after the 50th cycle. Results from a limited number of penetrometer readings at minimal joint width, or maximum compaction, are not reported here, as all readings exceeded the 500 kPa limit of the pocket penetrometer, indicating effectively a relative density above 80% during maximum compaction.

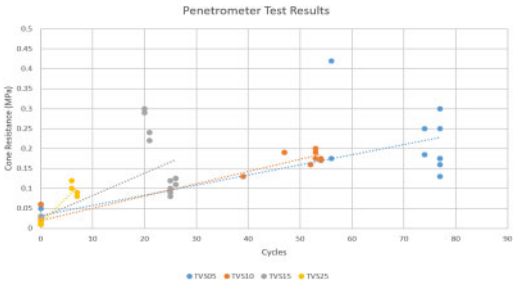

Figure 12. Penetrometer test results.

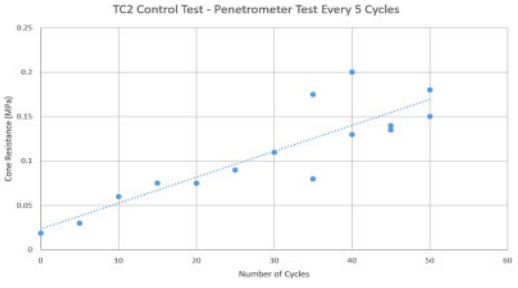

Figure 13. Stepwise penetrometer tests (TC2-XX) results.

Figure 13 plots the TC2 test results with a trend line drawn through. It is clear that cone resistance, and thereby relative density, steadily increases with each cycle.

4 CONCLUSIONS

The results of a series of compression-extension experiments of a model immersed tunnel joint gap show that the cyclic, seasonal, movement of the tunnel segments significantly increases the soil stresses in the joint. This increase in soil stresses occurs due to overlying sand entering the joint gap, where it is subsequently compacted. Penetrometer test results confirm that the sand in the joint gap increases in cone resistance, and therefore density, after subsequent loading and unloading cycle.

During each deformation cycle, the soil stresses in the joint are observed to increase. Also a cyclic deformation of the Gina gasket towards the inside of the tunnel is observed from LVDT readings, showing that these increasing soil stresses are also exerted onto the Gina gasket. However, during unloading the Gina gasket does not fully rebound, resulting in a gradual inward movement of the Gina, that can lead to its ultimate failure.

ACKNOWLEDGMENTS

The authors would like to express their gratitude to S. van Herk, C. van Beek, R. van Leeuwen and J.J. de Visser for their assistance during the design and construction of the setup, to J. van Stee and Trelleborg Netherlands BV for manufacturing a custom scaled Gina profile, and to the Municipality of Rotterdam for financial support of the first Author during this project.

REFERENCES

Berkhout, B. (2015). Instandhouding zinkvoegen. Technical report, COB.

Broere, W. (2001). *Tunnel Face Stability & New CPT Applications*. Ph. D. thesis, Delft University of Technology, Delft.

Broere, W. & A. van Tol (1998). Horizontal cone penetration testing. In P. Robertson and P. Mayne (Eds.), *Geotechnical Site Characterization, Proc. ISC'98*, pp. 989–994. Balkema.

COB Commissie T202 (2015). Handboek tunnelbouw. Technical report, COB.

Elmi Anaraki, K. (2008). Hypoplasticity investigated: Parameter determination and numerical simulation. Master's thesis.

Jamiolkowski, M. (2001). Evaluation of relative density and shear strength of sand from cpt and dmt. In D. Lo Presti and M. Manassero (Eds.), *LADD Symposium*.

Kulhawy, F. & P. Mayne (1990). Manual on estimating soil properties for foundation design. Technical Report EPRI-EL-6800, Electric Power Research Inst., Palo Alto, CA (USA).

Lunniss, R. & J. Baber (2013). *Immersed Tunnels*. CRC Press.

Sandrekarimi, A. (2016). Estimating relative density of sand with cone penetration test. *Ground Improvement 169*(4), 253–263.

Schmertmann, J. (1976). An updated correlation between relative density d_r and fugro-type electric cone bearing, q_c. Technical Report DACW 39-76, M 6646 WES, Vicksburg, Miss. (USA).